# A Numerical Model for the Evaluation of the Influence of Pavement Surface on the Microclimate

Vu Thanh Ca* and Takashi Asaeda**

### Abstract

Outdoor experiments and numerical analysis were carried out to investigate the effects of various pavement materials on the microscale thermal environment. It was found that the ceramic porous pavement, with small inside pores, can absorb a large amount of water after a rainfall or from the underlying soil. The water contained in the pavement is later evaporated and helps to keep the pavement surface temperature much lower than that of the normal porous pavement.

A numerical model of the large eddy simulation type was developed to study the impact of pavement samples on the micro scale thermal environment. The computational domain consists of a pavement surface with a building at its center. Computations were performed for two cases: the ground surface is covered by the asphalt pavement and the ground surface is covered by the ceramic pavement. Results of the computations reveal that the evaporation at the ceramic pavement surface is the most important reason for making its surface temperature lower than that of asphalt pavement. At 2 p.m., air temperature at 3.5m above the asphalt pavement is about 1.5K higher than that above the ceramic pavement. At 8 p.m., this difference is less than 1K.

Key words: permeable pavement, evaporation, microclimate, large eddy simulation

## 1   Introduction

Studies (Asaeda and Vu, 1993, Asaeda et al, 1996) revealed that at noon, surface temperature of asphalt pavement can reach more than 55°C, and the surface releases more than $350W/m^2$ and $600W/m^2$ to the atmosphere in the form of sensible heat and upward longwave radiation, respectively. The sensible heat directly heats the air, while the upward longwave radiation can increase the thermal load on pedestrians and cause great thermal discomfort.

The main reason for the increase in temperature at the surface of the normal impermeable pavement is the lack of evaporation, which for natural bare soil surface at its peak arround noon, can be as large as $400W/m^2$ and consumes a large portion of net radiation to the surface, thereby helping reduce the surface temperature. Due to intensive evaporation, the surface temperature of bare soil at noon is only around 40°C and decreases to lower than that of the air soon after sunset (Asaeda and Vu, 1993).

Thus, it is desirable that a kind of pavement which enables the exchange of water between the pavement and the underlying soil, and consequently enables the evaporation at the ground surface, be used in the urban area. Previous studies (Vu et al, 1996) found that among various porous pavement materials, ceramic porous pavement can be used for this purpose. However, the effects of this and other kinds of pavement on the below-canopy thermal climate has not been properly investigated.

Inagaki et al (1993) developed a two-dimensional model for the study of the wind, air temperature and humidity fields in a street canyon. The role of the plant in the street canyon on the distribution of wind velocity, air temperature and humidity was studied in this model.

This study presents preliminary attempts to investigate the heating and evaporation processes in the urban canopy, and the effects of different pavement materials on the urban canopy microclimate based on a numerical model. The Navier-Stokes equations, continuity equation, and equations of heat and moisture transfer in the air are solved using a Large Eddy Simulation (LES) technique coupled with appropriate boundary conditions for momentum, heat and moisture fluxes at the ground surface and walls and roofs of buildings.

*   Member, Faculty of Engineering, Saitama University
    Urawa, Saitama 338, Japan
*   Member, Graduate School of Science and Engineering, Saitama University
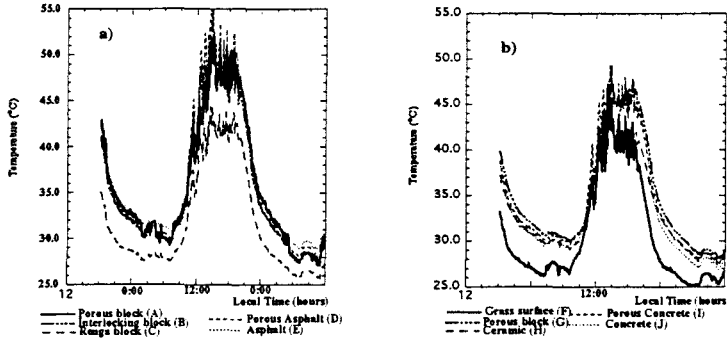    Urawa, Saitama 338, Japan

Figure 1: Surface temperature of various pavement samples on August 8-10, 1994

# 2 Field Experiment

Outdoor experiments were performed for the purpose of understanding the heating characteristics of various pavement materials. During the field experiment, temperature and ground heat flux at the surface and various depths below the surface of the pavements, together with meteorological conditions such as air temperature, relative humidity, wind velocity, solar radiation, downward longwave radiation, were recorded at 5 minutes interval continuously from August, 1994 to May, 1995. More information on the experiment can be found in Vu et al (1996).

Surface temperatures of various pavement samples measured during the extensive observation of 8-9 August, 1994 are depicted in Figs. 1 (a,b). At noon, surface temperature of the porous asphalt pavement reaches 52°C, which is almost the same as that of the normal porous block and 3°C lower than that of the asphalt pavement, which reaches 55°C. At the same time, the temperature at the surface of the ceramic pavement reaches only 42°C, almost the same as that of the natural grass surface.

The high surface temperature of the normal porous pavement can be explained by the effects of the pore size in pavement materials on the thermal behaviours of the pavement. The normal porous block, having a large pore size, can not keep the water inside and is dried up rapidly. This makes its surface temperature at noon as high as that of the normal impermeable concrete pavement. On the other hand, ceramic porous pavement, possessing small pore size can absorb a large amount of water during a rainfall and from the underlying soil. The water contained inside the pavement sample is later evaporated, which helps keep the temperature at the surface of the ceramic pavement much lower than that at the surface of other porous pavements.

# 3 Analysis of the Effects of Pavement on the Urban Micro-climate Based on a LES Model

In order to investigate the effects of heating and evaporation processes at the surface of the ceramic pavement on the urban microclimate, and with the purpose of understanding the heat and moisture transfer processes inside the urban canopy layer, a turbulent model of the Large Eddy Simulation (LES) type has been developed. The outline of the model is as follows

## 3.1 Governing Equations

A top-hat filter is applied to the Navier-Stokes equations, continuity equation and equations of heat and moisture transfer in the air. The three-dimensional filtered equations with the Boussinesq approximation, after non-dimensionalization, can be written in tensor form as follows:

$$\frac{\partial u_i}{\partial t} + (\omega \times u)_i = -\frac{\partial p}{\partial x_i} - \frac{\partial K}{\partial x_i} - \frac{\partial \tau_{ij}}{\partial x_j} + \frac{R_a}{P_r R_e^2}\delta_{i3}, \tag{1}$$

$$\frac{\partial u_j}{\partial x_j} = 0, \tag{2}$$

$$\frac{\partial \theta}{\partial t} + \frac{\partial}{\partial x_j} u_j \theta = -\frac{\partial}{\partial x_j} H_j, \tag{3}$$

$$\frac{\partial q}{\partial t} + \frac{\partial}{\partial x_j} u_j q = -\frac{\partial}{\partial x_j} Q_j, \tag{4}$$

where $u$ is the filtered velocity vector and $u_i$ are its components, $\omega$ is the filtered vorticity vector, $t$ time, $p$ filtered pressure, $\theta$ and $q$ are the filtered virtual potential temperature and mixing ratio, respectively; $K = |u|^2/2$ the mean kinetic energy, $\tau_{ij}$, $H_j$ and $Q_j$ are the subgrid scale (SGS) Reynolds stresses, heat and moisture fluxes, respectively; $R_e$ ($= Uh/\nu$) Reynolds number, $P_r$ the Prandtl number ($= \nu/\kappa$), $R_a$ ($= gh^3\Delta\theta/\nu\kappa_h\theta$) Rayleigh number and $\Delta\theta = \theta - <\theta>$ with $h$ a characteristic height, $U$ a characteristic velocity, and $\nu$ and $\kappa_h$ the kinematic viscosity and thermal diffusivity of the air, respectively. Here, the angle bracket $<>$ is used to denote the horizontally average values.

In the system of equations (1-4), velocity components are nondimensionalized by wind velocity $U$ at large height, length by a characteristic length $h$, the total height of the computational domain, which extends to 100m from the ground surface, virtual potential air temperature and mixing ratio by virtual potential air temperature and mixing ratio at the top of the computational domain $\theta_a$ and $q_a$, respectively.

The subgrid-scale (SGS) Reynolds stresses is defined as

$$\tau_{ij} = R_{ij} - \frac{R_{kk}}{3}\delta_{ij} \tag{5}$$

with

$$R_{ij} = \overline{u_i' u_j'} \tag{6}$$

The overbar in equation 6 represents the filter operation. The Smagorinski (1963) model is employed for the evaluation of the SGS Reynolds stress

$$\tau_{ij} = -2\nu_m S_{ij} \tag{7}$$

where the rate of strain tensor $S_{ij}$ is defined as

$$S_{ij} = \frac{1}{2}\left(\frac{\partial u_i}{\partial x_j} + \frac{\partial u_j}{\partial x_i}\right) \tag{8}$$

In this study, a modification of this model proposed by Deardoff (1980) and Moeng (1984) is used for the evaluation of the SGS eddy viscosity.

The SGS heat and moisture flux are evaluated as

$$H_j = -\nu_m \frac{\partial \theta}{\partial x_j} \tag{9}$$

$$Q_j = -\nu_m \frac{\partial q}{\partial x_j} \tag{10}$$

The instantaneous SGS eddy viscosity is evaluated following Moeng (1984), Deardoff (1980) as

$$\nu_m = c_s l k^{1/2}, \tag{11}$$

where $c_s$ is a constant, equal to 0.1; and $k$ is the SGS turbulence kinetic energy $k = \overline{u_i' u_i'}/2$. The prognostic equation for $k$ is as follows

$$\frac{\partial k}{\partial t} = -\overline{u_i \frac{\overline{\partial k}}{\partial x_i}} - \overline{u_i' u_j'}\frac{\partial u_i}{\partial x_j} + g\overline{w'\theta'} - \frac{\partial [\overline{u_i'(k+p')}]}{\partial x_i} - \varepsilon \tag{12}$$

In this equation, the gravitational acceleration $g$ is nondimensionalized by $U^2/h$. The closure assumptions made here in order to solve (12) are the downgradient diffusion assumption and the Kolmogoroff hypothesis.

## 3.2 Boundary Conditions and Solution Scheme

The boundary conditions at the ground surface for wind velocity are evaluated following Moeng (1984), i.e. using the similarity formula

$$\frac{\partial u}{\partial z} = \frac{u_*}{\kappa dz_1/2} \Phi_m \left( \frac{dz_1/2}{L} \right), \tag{13}$$

with $dz_1$ is the thickness of the first air layer above ground surface, as a non-staggered grid is used (Armfield, 1991), $u_*$ the local friction velocity at the ground surface whose direction is the same as that of the surface stress, and $\kappa$ the von Karman constant. The stability function $\Phi_m(\zeta)$ has the form (Businger et al, 1971)

$$\left. \begin{array}{ll} \Phi_m(\zeta) = (1 - 15\zeta)^{-\frac{1}{4}} & \text{unstable condition} \\ \Phi_m(\zeta) = 1 + 4.7\zeta & \text{stable condition} \end{array} \right\} \tag{14}$$

where $\zeta = z/L$ is the dimensionless height above the surface and $L$ is the Monin-Obukhov length.

The mean virtual potential temperature gradient near the ground surface is evaluated as

$$\frac{\partial \theta}{\partial z} = \frac{\theta_*}{\kappa dz_1/2} \Phi_h \left( \frac{dz_1/2}{L} \right), \tag{15}$$

and the mixing ratio gradient near the ground surface is evaluated as

$$\frac{\partial q}{\partial z} = \frac{q_*}{\kappa dz_1/2} \Phi_h \left( \frac{dz_1/2}{L} \right). \tag{16}$$

where $\theta_*$ and $q_*$ are the scales for virtual potential temperature and mixing ratio at the ground surface, respectively; $\theta_* = H/u_*$ and $q_* = E/u_*$ with $H$ as the sensible heat and $E$ as the evaporation rate at the ground surface. In Eqs. (18-19), the same stability function $\Phi_h$ is assumed for the heat and mass transfer at the ground surface. The form of the function $\Phi_h$ is (Businger et al, 1971)

$$\left. \begin{array}{ll} \Phi_h(\zeta) = 0.74(1 - 9\zeta)^{-\frac{1}{2}} & \text{unstable condition} \\ \Phi_h(\zeta) = 0.74 + 4.7\zeta & \text{stable condition} \end{array} \right\} \tag{17}$$

The local friction velocity at a solid surface element is defined as

$$u_* = (\tau_{in}^2 + \tau_{jn}^2)_0 \tag{18}$$

where $i$ and $j$ are directions parallel to, and $n$ is the direction normal to the solid surface; and the subscript 0 denotes values at the surface.

The SGS fluxes of momentum, heat and moisture at the solid surface are evaluated as in Moeng (1984) with the assumption of a constant drag coefficient over the surface under consideration

$$(\tau_{in})_0 = <\tau_{in}>_0 \frac{S_1 <u_{i1}> + <S_1> (u_{i1} - <u_{i1}>)}{<S_1><u_{i1}>} \tag{19}$$

$$(H_n)_0 = <H_n>_0 \frac{S_1(<\theta_1> - \theta_0) + <S_1> (\theta_1 - <\theta_1>)}{S_1(<\theta_1> - \theta_0)} \tag{20}$$

$$(Q_n)_0 = <Q_n>_0 \frac{S_1(<q_1> - q_0) + <S_1> (q_1 - <q_1>)}{S_1(<q_1> - q_0)} \tag{21}$$

where $S_1 = (u_{i1}^2 + u_{j1}^2)^{1/2}$ is the wind speed, and subscript 1 denotes the values at the first grid points outside the solid surface. The angle bracket in Eqs. (19-21) denotes the average in the directions parallel to the solid surface.
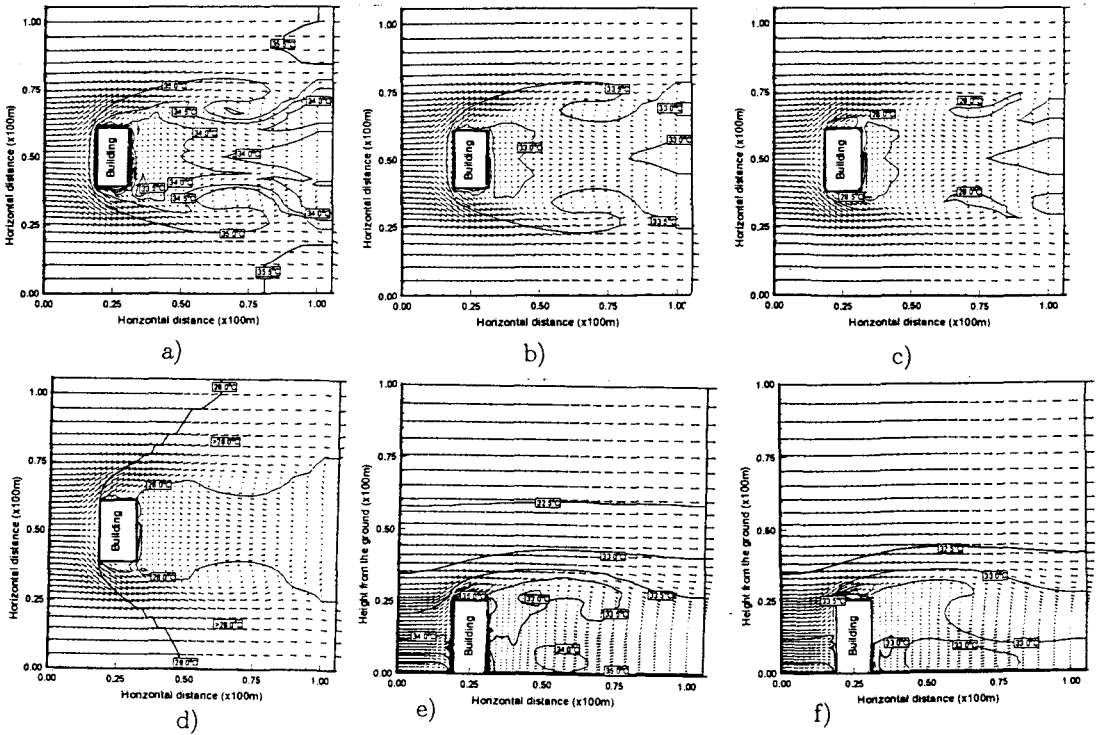
Figure 2: Horizontal air temperature and wind velocity at 3.5m above the surface of a) asphalt pavement (2 p.m.), b) ceramic porous pavement (2 p.m.), c) asphalt pavement (8 p.m.), d) ceramic porous pavement (8 p.m.); and air temperature and wind velocity distribution at a vertical cross-section at the center of the computational region at 2 p.m. for the case of e) asphalt pavement surface, and f) ceramic pavement surface

Strictly speaking, temperature at the ground surface, walls and roof of the building should be properly computed by the solutions of the one dimensional heat conduction equation for walls, roof or impermeable pavement, and the coupling of subsurface heat and moisture transfer for the permeable pavement. However, it may take several hours of real time from the beginning of the computation for the walls, roof or ground surface to change their temperature and eliminate the influence of the initial condition. Due to computer limitation, computation for such a long time is still not possible in this study. Thus, temperatures of roof, walls of building and ground surface are given from the results of a static pressure model for the canopy layer.

A common assumption for the boundary conditions for the large eddy simulation of the planetary boundary layer is that of periodic boundary conditions in the horizontal directions. However, with the complex geometry in the urban area, the wind velocity, air temperature and moisture at the downwind boundary is very different from that at the upwind boundary, and periodic boundary conditions can not be applied. With this in mind, zero normal gradients of velocity components across the downwind, lateral and upper boundaries are assumed.

At the upwind boundary, a turbulent velocity distribution profile in the vertical direction is specified. For the heat and moisture transfer equations (3-4), zero normal gradients of air temperature and mixing ratio are specified at all horizontal open boundaries, and given free atmospheric temperature and mixing ratio at the upper boundary.

The system of equations (1-4) for the wind velocity, air temperature and vapor density fields was discretized in finite volume form on a non-uniform, non-staggered grid (Armfield, 1991). Pressure is computed using the SMAC method.

In general for the simulation of three dimensional turbulence using a *LES* model the grid size should lie in the inertial sub-range. This requirement is somewhat relaxed in the present model in which the subgrid scale kinetic energy is computed explicitly, and thus an equilibrium assumption is not required, as noted by Moeng (1984). Nonetheless a relatively fine grid is still required, and the results presented here have been obtained on a 37(lateral) × 38(logitudinal) × 44(vertical) mesh. It should be noted that at this preliminary stage of the investigation detailed grid dependency checks have not been carried out

due to the limitations in available computer. The corresponding time step is 0.2s.

Initial conditions for the air temperature , wind velocity, wall and ground surface temperature are obtained from those computed using a static pressure model reported in Vu et al (1995).

## 3.3    Results and Discussions

Figs. 2(a-d) depict the horizontal distributions of air temperature and wind velocity at 2 p.m. and 8 p.m. for asphalt and ceramic pavements, respectively. Figs. 2(e,f) depicts the air temperature and wind velocity distribution at a vertical cross-section at the center of the computational region at 2 p.m. for asphalt and and ceramic pavements, respectively.

The model used here, even on the present mesh, is providing a qualitatively accurate prediction of the dominant features of the flow, that is the size and location of the recirculation region downstream of the building, as identified in Murakami (1991) in which the results of a series of wind-tunnel experiments, and numerical simulations using a $k - \epsilon$ model and a large eddy simulation model, were reported.

In general the flow is characterised by the repeated formation and shedding of eddies at the downstream edges of the building. These eddies are predominantly a result of the wind shear, as a strong wind of 2 m/s is assumed in the computation; and are little influenced by buoyancy. Thus little difference is seen in the flow fields for the different cases, even though there is a variation in the temperature field.

From Figs. 2(a-d) it can be seen that hot regions in the flow are formed at the outer edges of the building and wake, as a result of the evolution of the eddies which result in an upward flow of air in these regions. The centre of the downstream wake is subjected to a downward flow of air, as can be seen in Figs. 2(e-f), which acts to cool this region of the wake.

At noon the air temperature 3.5$m$ above the surface is overall about 1.5K hotter for the asphalt pavement than for the ceramic pavement, with the greatest difference being 2K in the hottest region at the outer edges of the building (Figs. 2, a-d). At 8pm this difference is reduced to less than 1°K, with the temperature field for the ceramic pavement being almost homogeneous at this height and time, indicating that the ceramic pavement has now cooled and is in equilibrium with the air.

The vertical cross sections (Figs. 2, e-f) show that hot regions are located near both the building roof and, for both the asphalt and ceramic pavements, near the ground surface. However it is also seen that the temperature near the ceramic pavement is about 2°K cooler than that near the asphalt pavement.

It is thus clear that the model used here is able to provide a qualitatively accurate prediction of experimentally observed difference in heat transfer and thermal properties of asphalt and porous ceramic paving materials. Further work is required to fully validate the model, in particular grid and time step dependency tests must be carried out, while additionally detailed comparisons with wind tunnel results that are currently being collected will be carried out.

# References

Armfield S.W. (1991) *Computers Fluids.* **20**, 1-17.

Asaeda T., and Vu T. C. (1993) *Boundary-Layer Meteorol.*, **65**, 159-179.

Asaeda T., Vu T. C. and A. Wake (1996) *Atmospheric Environment,* **30**, 413-427.

Businger J.A., J.C. Wijngaard, Y.I. Izumi and E.F. Bradley (1971) *J. Atmos. Sci.*, bf 28, 181-189.

Deardoff J.W. (1980) *Boundary-Layer Meteorol.*, **48**, 495-527.

Inagaki S., M. Hino, M. Kanda (1993) *Annual Journal of Hydraulic Engineering, JSCE,* 37 355-360.

Moeng, C.H. (1984) *J. Atmos. Sci.*, **41**, 2052-2062.

Murakami S., A. Mochida, Y. Hayashi and K. Hibi (1991) *Energy and Building*, **15-16** (1990/91) 345-356.

Smagorinsky J. (1963) *Monthly Weather Review .* **91**, 99-164.

Vu T.C., T. Asaeda, T. Fujino and M. Murakami (1995) *Environmental System Research, JSCE*, Vol. 23, 223-228.

Vu T. C., T. Asaeda and M. A. Eusuf (1996) *Annual Journal of Hydraulic Engineering, JSCE*, 449-454.